Higher-Order 3D-Shell Elements in LS-DYNA – Enhancing Stress Prediction in Laminates

Maximilian Schilling[1], Malte von Scheven[1], Manfred Bischoff[1]

[1]University of Stuttgart, Institute for Structural Mechanics,
Pfaffenwaldring 7, 70569 Stuttgart

1 Abstract

Accurate stress prediction in fiber-reinforced laminates is crucial for anticipating damage like delamination in lightweight designs. While standard Reissner–Mindlin shell elements are computationally efficient for large-scale explicit simulations, they are inaccurate due to simplifying assumptions like zero transverse normal stress and straight cross-sectional fibers. Conversely, fully three-dimensional solid element discretizations, while accurate, are computationally prohibitive for industrial-size models. This contribution presents the application of higher-order 3D-shell elements, implemented as a user-defined element in Ansys LS-DYNA, to bridge this gap. Unlike standard shells, these higher-order 3D-shell elements can capture cross-sectional warping and a higher-order strain distribution in the transverse direction, providing a fully three-dimensional stress state.

Through a variety of comparative analyses against standard Ansys LS-DYNA shell elements, our studies demonstrate significantly improved stress prediction for the higher-order 3D-shell elements. This includes a substantially more accurate prediction of all stress components in a detailed analysis of a laminate but also for larger-scale simulations like the simulation of a split disk test. The simulation results from the higher-order 3D-shell elements align closely with detailed stress distributions from fully three-dimensional solid simulations yet maintain a significant computational advantage. These studies utilize a three-dimensional orthotropic material model for all benchmark simulations.

In conclusion, our contribution highlights a promising and viable approach to achieve more reliable stress predictions for composite structures in Ansys LS-DYNA, crucial for robust design and damage assessment, without the prohibitive cost of fully three-dimensional discretization.

Keywords: higher-order 3D-shell elements, fiber-reinforced laminates, stress prediction

2 Introduction

Fiber-reinforced composite materials are composed of higher-stiffness fibers embedded in a lower-stiffness matrix. These materials are categorized by their matrix type (polymers, metals, ceramics), fiber type (carbon, glass, aramid), and reinforcement geometry (short or continuous fibers). This contribution focuses on continuous carbon-fiber reinforced polymer (CFRP) laminates. These laminates consist of layers of unidirectional, continuous carbon fibers embedded in a polymer matrix. The fibers of each layer can be oriented independently of all other layers, allowing the stiffness of the resulting component to be tailored. For a comprehensive overview of fiber-reinforced composites in general, readers are referred to Mallick [1].

Due to their tailorable properties and high stiffness-to-weight ratio, fiber-reinforced laminate structures are widely used in lightweight design. In the automotive context, they are, for example, utilized for structural members, car body components, and pressure tanks in hydrogen-powered vehicles. However, due to their orthotropic, layerwise material properties with abrupt changes in stiffness, these materials exhibit heterogeneous three-dimensional stress states and brittle, multimodal failure mechanisms.

The lower safety margins in lightweight design and the intricate material behavior necessitate accurate numerical modeling to predict the structural behavior and these failure modes. In this context, an accurate prediction of the stress distribution is of utmost importance, as stress serves as the input for most failure models. For this, finite element simulations are used, utilizing different modeling approaches. As most laminated structures are manufactured as shell-like structures, computationally

efficient Reissner–Mindlin shell finite elements are often employed. While computationally efficient, they offer only limited capabilities to correctly predict the complex stress state in a laminate due to their underlying kinematic assumptions, particularly for transverse normal stress, transverse shear stress, or free-edge stress concentrations. This results in a low accuracy of the distribution of the transverse stress components over the thickness coordinate of the laminate, as shown, for example, by Främby et al. [2], which can compromise the reliability of failure predictions. Other research by Czichos et al. [3] also emphasizes the importance of predicting the complex, fully three-dimensional stress state, particularly in impact scenarios. Therefore, the applicability of Reissner–Mindlin shell finite elements to the simulation of fiber-reinforced laminates is limited. While more sophisticated shell models exist, they currently play a minor role in the simulation of laminated composites and will be discussed later on. If a high-fidelity simulation of laminated components is needed, stacked solid elements, sometimes in combination with cohesive zone elements, are used. This allows an accurate prediction of the complete, fully three-dimensional stress state. Especially in time-explicit finite element simulations, as they are often conducted in Ansys LS-DYNA, this is numerically very expensive due to the small time step of the stacked solids.

One current limitation in the simulation of fiber-reinforced laminates, therefore is the absence of a modeling approach that offers predictive capabilities for stress comparable to stacked solid elements but offers the numerical efficiency of a shell formulation. Especially the shortcomings of shell elements, namely the prediction of a reduced stress state only and the limitations due to underlying kinematic assumptions, need addressing.

This study investigates the potential of using 3D-shell elements with higher-order through-the-thickness kinematics to overcome these challenges. The element formulation employed in this contribution was developed by Willmann [4] for sheet metal forming applications with the aim to obtain an improved resolution of the stress distribution in comparison to standard shell finite elements. The objective of our research is to investigate the effectiveness of these elements to improve the stress prediction for fiber-reinforced laminate structures while maintaining computational efficiency.

In this work, we evaluate the predictive capabilities of higher-order 3D-shell elements by systematic comparative analyses with the standard modeling approaches for two different simulation scales. First, a simulation of a laminate detail will be conducted to evaluate the capabilities of the approaches to capture stress concentrations on free edges. Secondly, a larger-scale split ring test will be investigated to compare the predictions for a component-level simulation. For each simulation we compare the stress results from higher-order 3D-shell element simulations with those of standard shell element simulations and with those of fully three-dimensional solid element simulations. With these more complex scenarios on different scales, this contribution builds upon the article by Schilling et al. [5], providing an indication for more possible applications of the higher-order 3D-shell elements.

The contribution is structured as follows: Chapter 3 describes shell models and finite elements currently used in state-of-the-art simulations in Ansys LS-DYNA and their application to fiber-reinforced laminate structures. Furthermore, an overview over the higher-order 3D-shell model by Willmann [4] is given. Chapter 4 follows with an overview of the conducted numerical studies and the comparison of stress results for different simulation models for laminated structures. Chapter 5 summarizes the contribution and provides an outlook on possible investigations in the future.

3 Shell finite elements and their application to laminates

Accurate numerical modeling of fiber-reinforced laminate structures requires element formulations that balance computational efficiency with the ability to capture complex three-dimensional stress states. This section reviews the modeling approaches commonly employed in state-of-the-art simulations of laminated composites, with a focus on the shell elements and solid elements available in Ansys LS-DYNA. For this, we give an overview of the underlying shell models, highlighting their kinematic assumptions and resulting limitations for laminates. From each presented shell model, one representative shell element in Ansys LS-DYNA is chosen and used for the numerical simulations. Lastly, we introduce the higher-order 3D-shell formulation developed by Willmann [4], which we will compare against state-of-the-art modelling approaches in this work. A comprehensive review of shell models is given by Bischoff et al. [6].

3.1 Reissner–Mindlin shell elements

The most widely used shell finite elements are formulated on the basis of the Reissner–Mindlin shell model. Amongst others, the model relies on the assumptions of straight transverse fibers remaining straight during deformation and transverse normal stress being zero. Moreover, there is no kinematic description of strain in the transverse direction. While these assumptions are reasonable and enable efficient computation for many applications, they are less valid for laminated materials. In laminates, initially straight transverse fibers may bend due to stiffness differences between the layers and significant transverse normal stress can occur, particularly at free edges. Consequently, these assumptions limit the accuracy of Reissner–Mindlin shell elements in predicting stress distributions in laminates.

In LS-DYNA, the shell elements of **`ELFORM=2`** (in the following 'Shell 2') or **`ELFORM=16`** are examples of shell elements derived from this model [7]. In the following, Shell 2 proposed by Belytschko, Lin, and Tsay [8] is used as a representative for Reissner–Mindlin shell elements.

For completeness, there exist some higher-order shear deformation theories, for example, by Carrera et al. [9]. But as elements based on these theories are not widely used, not implemented in Ansys LS-DYNA, and also still only offer the prediction of a reduced stress state, they are not discussed further in this contribution.

3.2 Shell elements with thickness stretch

In comparison to Reissner–Mindlin shell elements, shell elements with a thickness stretch include a change of thickness and transverse normal stress in their underlying model. They can predict the fully three-dimensional stress state and are therefore also called 3D-shell elements. As a result, the same three-dimensional material laws as with solid elements can be used. While shell elements with thickness stretch offer greater predictive capabilities due to their enhanced kinematics, they are still limited by straight transverse fibers remaining straight. The transverse normal strain can also only be predicted up to linear order. Several publications proposed this shell model independently, most notably Kühhorn and Schoop [10] and Parisch [11]. However, these elements still struggle to accurately capture the complex stress states in laminates, particularly in scenarios involving significant cross-sectional warping or non-linear transverse stress distributions.

In LS-DYNA, the shell elements of **`ELFORM=25`** (in the following 'Shell 25') or **`ELFORM=26`** are examples of shell elements derived from this model [7]. In this contribution, Shell 25 is used as a representative for shell elements with thickness stretch.

3.3 Higher-order 3D-shell elements

In contrast to these shell elements, a higher-order 3D-shell element includes additional degrees of freedom, allowing a higher-order warping of its transverse fibers and a higher-order strain field with respect to the (transverse) thickness coordinate. In Figure 1 deformation modes of the transverse fibers of a higher-order 3D-shell element are depicted up to cubic order. Like shell elements with thickness stretch, it also considers a fully three-dimensional stress state.

In the following, a higher-order 3D-shell element allowing for up to cubic deformations of its transverse fibers (in the following '3DSH-cub') developed by Willmann [4] will be used. For a complete description of the family of higher-order 3D-shell elements and the implemented element technologies to prevent various locking phenomena, we refer to Willmann [4]. The element technologies include using reduced integration techniques and hourglass stabilization, the assumed natural strain method, and an additional incompatible quartic strain field in the transverse direction.

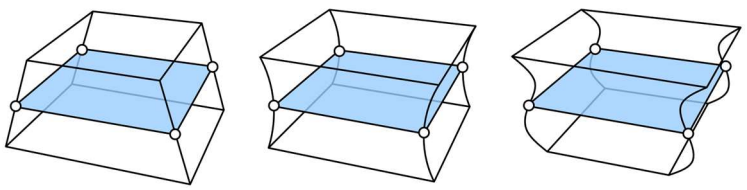

Fig.1: Visualization of linear, quadratic, and cubic deformations of the transverse fibers of a higher-order 3D-shell element, reprinted from [5] (open access).

Originally, this higher-order 3D-shell element formulation was developed for sheet metal forming applications, where thinning effects, cross-sectional warping effects, and the prediction of complex three-dimensional stress states are of high interest—but could not be resolved in industrial-scale simulations so far. For these types of simulations, the higher-order 3D-shell element offers an improved prediction of deformation and stress; see, for example, Wessel et al. [12] or Schilling et al. [13]. In contrast to this, the simulation of laminates is a non-smooth problem in the transverse direction due to the discrete layers. But due to these discrete layers with different material properties, also for these materials, complex three-dimensional stress states arise, for which we assume that they can be captured more accurately by these higher-order 3D-shell elements.

3.4 Application of shell elements to laminates and transverse integration rule

Lastly, we briefly address which options exist to model laminated structures with shell elements. In general, two distinct approaches exist: layers of the laminate can be represented either both in the kinematics of the shell element and the material model, or in the material model only. In both approaches, the number of integration points in the transverse direction is a multiple of the number of layers of the laminate. The integration points are then assigned the material properties of the respective layer. If the kinematics of the shell are enhanced, additional degrees of freedom are necessary—up to some additional degrees of freedom for each layer of the laminate that allow the independent rotation (and stretch) of transverse fibers in each layer. For the second approach, the shell element formulation remains unchanged and uses the standard kinematics of its underlying model. Only the integration points in the transverse direction are assigned different material properties, which affects the stress calculation for each layer. For details, we refer to the **`*SECTION_SHELL`** keyword and the respective **`ICOMP`** variable in the Ansys LS-DYNA User's Manual [7].

In this contribution, we use the second approach—standard kinematics with different material properties at the integration points in the transverse direction—for all simulations with shell elements, as the first approach is not implemented in LS-DYNA due to its higher complexity and increased numerical cost.

With respect to the integration rule of the shell elements in the transverse direction, there are some particularities for laminated materials. Usually, shell elements employ a Gauss integration rule in the transverse direction of the element. At least one integration point per layer of the material is used to represent each layer in the calculation of the structural response. But this integration rule uses variable weights, which would correspond to different layer thicknesses in the simulation. To represent equal layer thicknesses, as is often the case for laminated materials, an integration rule with equal weights is employed. For reference, see the **`*INTEGRATION_SHELL`** keyword in the Ansys LS-DYNA User's Manual [7]. While all integration points have the same weight, it is still possible to use multiple integration points per layer to achieve a more accurate evaluation of stress.

For the cubic 3D-shell elements investigated in this contribution, first investigations indicate that the stress prediction can be improved even further than just using multiple integration points per layer. Instead of using equal weights, each layer of the laminate can be integrated using a lower-order Gauss integration rule. We call this a 'composite Gauss integration' in the following. An example for this is given in Figure 2 for a six-point integration of a shell element consisting of two laminate layers. The equal-weight integration point positions are depicted as squares, while the integration point positions for a composite Gauss integration with three integration points for each layer are shown as triangles. Still, for both integration rules, the resulting layer of the laminate has same thickness, and the numerical expense is the same. Extensive studies on the influence of the thickness integration rule and possible positive effects on the accuracy of stress results still need to be conducted, especially for the higher-order 3D-shell elements. For both benchmark tests in this contribution, we specify the integration rule used for each element type. The comparison of stress is done for integration points with an identical thickness coordinate ζ, for example at $\zeta = 0.5$ in Figure 2.

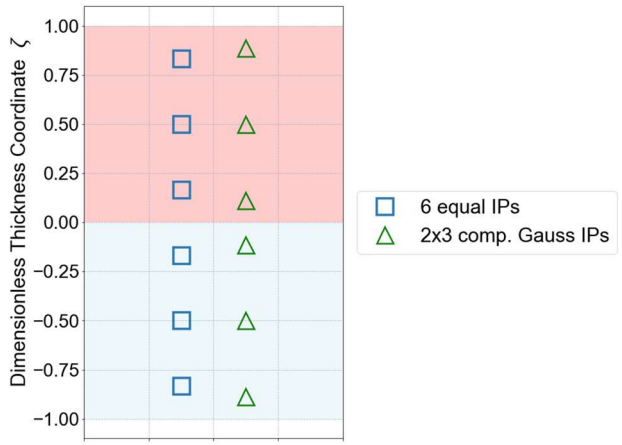

Fig.2: Comparison of integration point positions for two thickness integration rules of a two-layer laminate: equal-weight integration (squares) and composite-Gauss integration (triangles).

4 Stress analysis of laminated structures

In Chapter 4, we investigate the applicability of cubic 3D-shell elements for the stress analysis of laminated structures for two types of laminate analyses. An accurate prediction of the complex three-dimensional stress states in laminates is crucial for predicting damage and preventing premature structural failure. The two benchmark tests conducted complement a previous contribution [5], from which they branch in opposite directions. Of the two benchmark tests, one is focused on a very detailed stress analysis of a laminate section, with a particular emphasis on the phenomenon of stress singularities on free edges of laminates. The second benchmark test focuses on the stress prediction for a larger-scale simulation in the context of material testing for hydrogen pressure vessels.

We compare the simulation results obtained using Reissner–Mindlin shell elements (Ansys LS-DYNA Shell 2 [7]), shell elements with a thickness stretch (Shell 25 [7]), and those from our higher-order 3D-shell elements (3DSH-cub) with a reference solution obtained from a fully three-dimensional simulation employing stacked solid elements (Solid 1 [7]).

To model the layer-wise properties of a laminate, we assign orthotropic material properties rotated by the fiber angle β for each layer through the thickness of the laminate. In the case of the solid elements, the different material properties are assigned elementwise through the thickness of the laminate. Each layer of the laminate is represented by at least two solid elements in the transverse direction and therefore by at least two integration points. For the simulations with shell elements, the material properties are assigned to the integration points in the transverse direction of the elements. In this case too, at least two integration points are used per layer of the laminate.

To achieve a reference solution of high fidelity, the number of solid elements used through the thickness in the reference solution is always the same or larger than the number of integration points in the shell elements.

In order to ensure the feasibility of the conducted simulations, certain simplifications are made. We employ the orthotropic material model **`*MAT_022`** / **`*MAT_COMPOSITE_DAMAGE`** [14] and exclude damage for both benchmark simulations. Both in-plane damage and out-of-plane damage can be included in subsequent analyses in the future.

4.1 Free edge stress prediction

In the first benchmark, the mechanical response of a carbon fiber laminate of length l, width b, and thickness $t = 4\,\mathrm{mm}$ under tensile loading is investigated. This benchmark is proposed by Pagano [15] to showcase weaknesses of previous laminate theories in predicting the complex stress fields in composite laminates, with a focus on stress concentrations at free edges. The problem setup and the simulated system are illustrated in Figure 3 (left). During the simulation, the specimen is clamped at the

y-z-plane (red), and a displacement $\Delta u = 0.0183\,\mathrm{mm}$ is applied in x-direction at all nodes on the laminate edge highlighted in light blue. The laminate is composed of four layers of identical thickness h. The fibers in these layers are oriented at $\beta^{\uparrow} = \{45°, -45°, -45°, 45°\}$ (bottom to top) relative to the x-direction. Due to the different fiber orientations and the non-zero Poisson's ratio of the material, stress concentrations at the free edges of the laminate are expected. The chosen material properties for the carbon-fiber composite material are provided in Table 1 in the Appendix.

Three modelling approaches using shell elements are compared against a reference solution. These are Reissner–Mindlin shell elements (Shell 2), shell elements with thickness stretch (Shell 25), and higher-order 3d-shell elements (3DSH-cub). A simulation with nine solid elements (Solid 1) for each layer through the thickness of the laminate (36 elements in total) serves as the reference and is depicted in Figure 3 (left). Each solid element is cube-shaped with an edge length $e = 0.\overline{1}\,\mathrm{mm}$. For the simulations with shell elements, only one shell element is used in the transverse direction for the complete laminate. The shell elements use the same in-plane dimensions of $e = 0.\overline{1}\,\mathrm{mm}$ as the solid elements. All simulations were conducted using the central difference method for explicit time integration and no mass scaling.

While the solid elements use one integration point per element but are stacked, 36 integration points are used in the transverse direction for the solid reference simulation. All shell element formulations use 20 integration points in transverse direction, as this is the limit for the number of thickness integration points of the current implementation of the higher-order 3D-shell element. The Ansys LS-DYNA shell elements Shell 2 and Shell 25 use 20 integration points with equal weights, while the higher-order 3D-shell element 3DSH-cub uses a five-point composite Gauss integration for each layer for increased numerical accuracy and stability. This is depicted in Figure 3 (right). The stress components are compared at $\frac{h}{2}$ of layer 3 of the laminate, where every element formulation has an integration point. A comparison to the analytical results by Pagano is also possible, but omitted here to focus on an analysis of the complete stress state and all stress components, as Pagano focused only on selected stress distributions at certain locations.

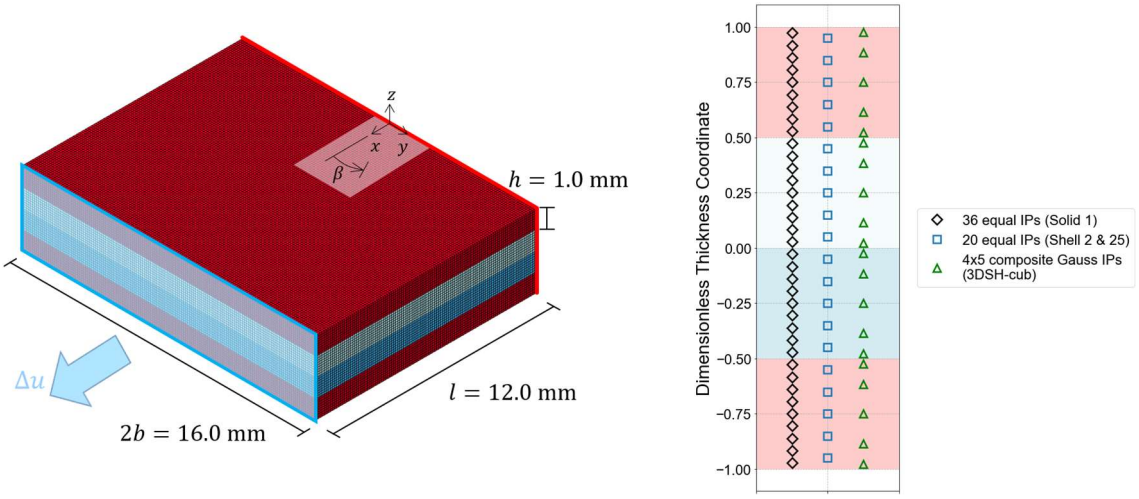

Fig.3: Stacked solid elements simulation setup of the tensile test by Pagano [15] (left); position of the thickness integration points for the different element formulations (right).

Figure 4 depicts the von Mises effective stress $\sigma_{\mathrm{v,M}}$ result of the reference simulation with stacked solid elements and is intended to showcase the complex stress state inside a simple laminate under uniaxial tension. Especially stress concentrations at layer boundaries at the free edges and at the laminate corners are prominent. The stress at the corners arises mostly from in-plane normal stress and normal stress in the transverse direction, while the stress concentrations between the layers at the free edges arise from in-plane shear stress. The following comparison investigates how well the different shell finite elements can capture this complex, three-dimensional stress state.

In Figure 5 we compare the distribution of stress at $\frac{h}{2}$ of layer 3 of the laminate for all in-plane and out-of-plane stress components. In the in-plane normal stress components (σ_x and σ_y), the solid reference solution exhibits stress concentrations in the direction of the fibers. For the normal stress σ_x the stress

visibly decreases in the direction of the free edges at $y = \pm b$ and the corners perpendicular to the fiber direction. The Shell 2 and Shell 25 formulations, however, reproduce these components only in a manner constant across the whole domain, overestimating the stress on the free edges while simultaneously underestimating the stress in the center of the laminate. In contrast, the 3DSH-cub element is able to reproduce the qualitative shape of the stress distribution due to its higher-order kinematics but with just a fraction of the degrees of freedom of the stacked solids at each in-plane nodal position (14 vs. 111). For the 3DSH-cub shell element, some local oscillations are visible, particularly at the free edges of the laminate at $y = \pm b$. The results for the normal stress σ_y are very similar, only for a smaller magnitude of stress. The cause of these oscillations still needs to be investigated in detail.

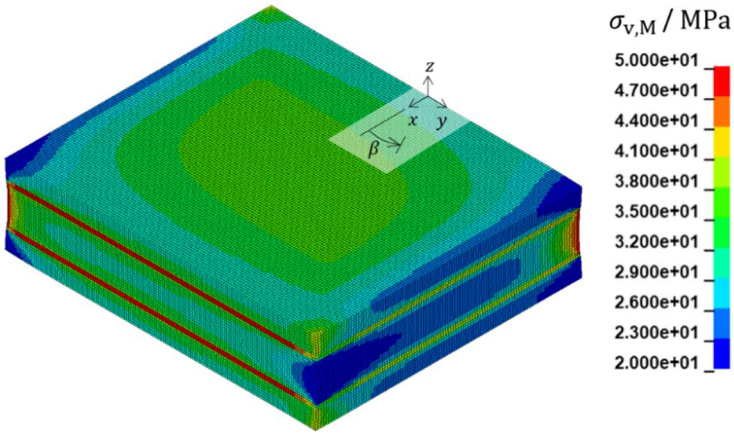

Fig.4: Effective stress $\sigma_{v,M}$ simulation result of the tensile test by Pagano [15] simulated with 36 stacked solid elements; displacements are scaled 50×.

For the transverse normal stress σ_z, the solid solution shows stress concentrations at the four corners of the laminate, arising from the non-zero Poisson's ratio and the different orientations of the fibers in the layers. Both shell formulations available in Ansys LS-DYNA are unable to predict any normal stress σ_z. Especially for Shell 25, this might be surprising, as this element formulation includes the calculation of thickness stretch and the transverse normal stress σ_z. The limitation of this element lies in its capability to only predict a linear thickness strain. For this benchmark, the total thickness of the laminate does not change, as two of the layers are stretched and two are compressed. These local variations of the normal strain in the transverse direction cannot be captured by Shell 25 which results in the prediction of zero transverse normal stress σ_z at the corners. In contrast, the 3DSH-cub element predicts a transverse normal stress distribution and magnitude very close to the reference solution due to the inclusion of transverse strain up to fourth order.

The shear stress components ($\tau_{xy}, \tau_{zy}, \tau_{zx}$) furthermore highlight the limitations of the standard shell formulations. The solid reference solution displays stress variations across the laminate; for example, for the in-plane shear stress τ_{xy} the reference solution shows compression in the center of the laminate while having stress-free edges. Both Shell 2 and Shell 25 fail to reproduce this variation, instead yielding uniform compression. The 3DSH-cub element provides a closer approximation of this distribution but cannot fully capture the stress-free condition. The higher-order 3D-shell element also again suffers from minor oscillations that deviate from the reference solution but overall achieves a stress prediction much closer to the reference.

Overall, this comparison demonstrates that while the shell formulations (Shell 2, Shell 25) reproduce the magnitude of the normal stress σ_x reasonably well, they are unable to capture the detailed distribution that arises in laminates. This is also the case for the two other in-plane stress components σ_y and τ_{xy}. All out-of-plane stress components cannot be captured at all by these standard shell elements, also not by Shell 25, which includes the calculation of thickness strain and the transverse normal stress σ_z. The higher-order 3D-shell formulation 3DSH-cub, on the other hand, shows much better capability in reproducing the variations of all stress components qualitatively, especially for the out-of-plane components. Some spurious oscillations still reduce accuracy and stem most likely from the much lower number of degrees of freedom and the effort to approximate a non-smooth function (discrete stiffness jumps between layers) with smooth polynomials. Further investigations to reduce these oscillations are possible.

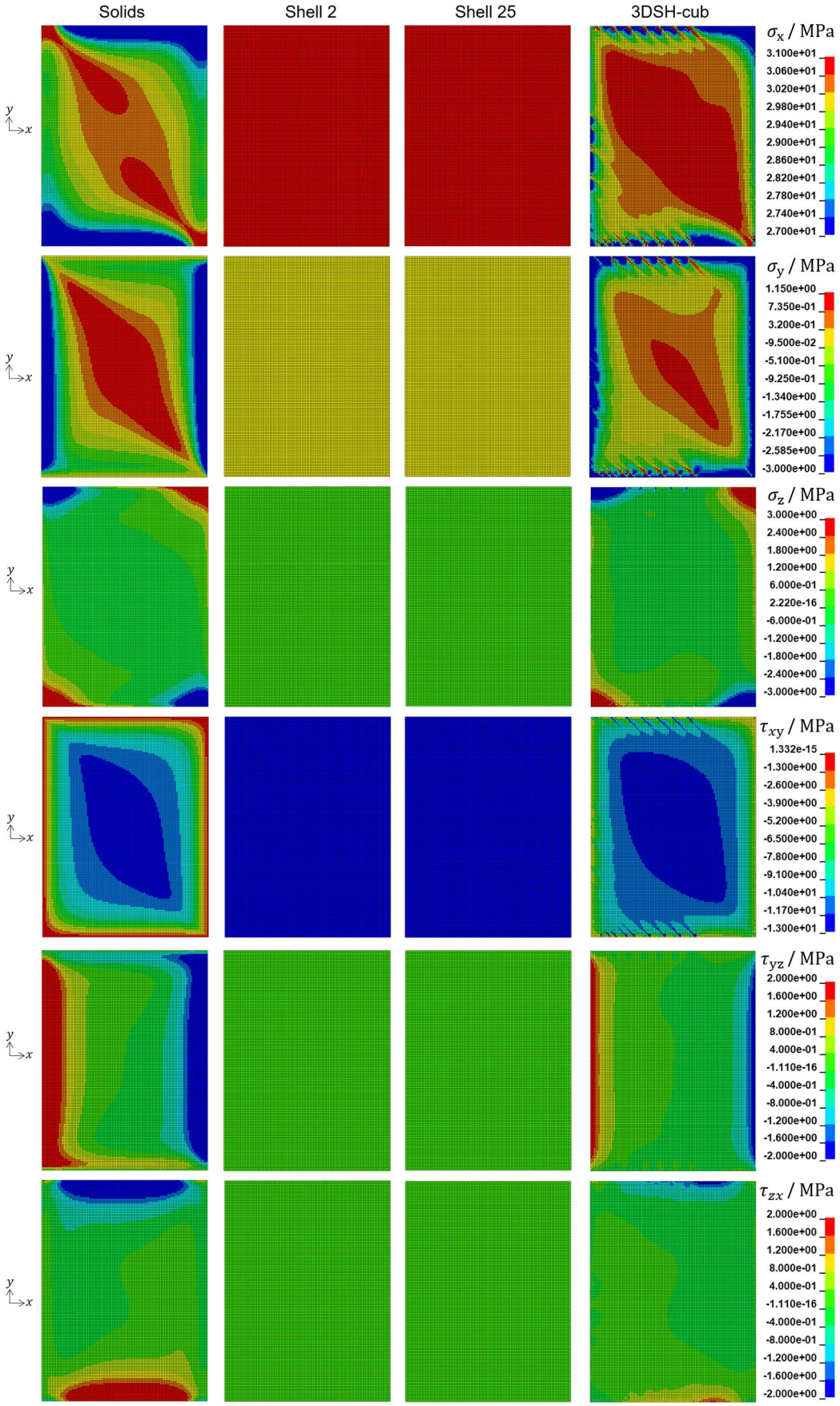

Fig.5: Comparison of all stress components for the tensile test by Pagano [15] for four different element formulations evaluated at $\frac{h}{2}$ of layer 3 ($\beta = -45°$).

4.2 Split disk test

In the second benchmark, the stress distribution in a carbon fiber laminated cylindrical ring under tension is analyzed. The purpose of the benchmark is to evaluate the stress prediction capabilities of the simulation approaches in a scenario of practical relevance, based on a standard test to measure the hoop strength of (reinforced) plastic pipes (ASTM D2290-19a) [16]. An eight-layer laminate ring with diameter d, width b, and thickness t is analyzed—the fiber orientations with respect to the circumferential direction $\beta^{\uparrow} = \{14°, -14°, 60°, -60°, 14°, -14°, 60°, -60°\}$ (inside to outside) are based on a hydrogen pressure vessel. On the inside of the laminate ring, two rigid semi-rings of diameter $d_i = 69.8\,\mathrm{mm}$ are located, of which the one in the negative 3-direction is fixed in all directions. These represent the split disks of the standard test. In Figure 6, the simulation setup is depicted, highlighting the refined mesh near the equator of the ring. For loading, the upper semi-ring is moved in the positive 3-direction by $\Delta u = 0.34\,\mathrm{mm}$, resulting in a tensile strain $\varepsilon_3 = 0.175\,\%$. The material properties of the simulation are specified in Table 2 in the Appendix.

Again, three modelling approaches using shell elements are compared against a reference solution. These are Reissner–Mindlin shell elements (Shell 16), shell elements with thickness stretch (Shell 25), and higher-order 3d-shell elements (3DSH-cub). Each shell element uses 8×2 Gauss integration points in the transverse direction, a two-point Gauss integration per layer of the laminate. A simulation with two solid elements for each layer through the thickness of the laminate (16 elements in total) serves as the reference and is depicted in Figure 6. The simulation results from this solid mesh are not fully converged, but the chosen discretization adheres to computational constraints and complies with industrial standards. All simulations were conducted using the central difference method for explicit time integration and no mass scaling.

The evaluation of the normal stress in the 3-direction around the equator of the ring is depicted in Figure 7 as a contour plot for two different layers of the laminate. The top row in the figure shows the stress distributions in layer 3 of the laminate, at integration point 6, and the bottom row shows the stress distributions in the outmost layer—layer 8, at integration point 16. The small discrepancy between the integration point position between the shell elements and the solid elements is neglected for these evaluations.

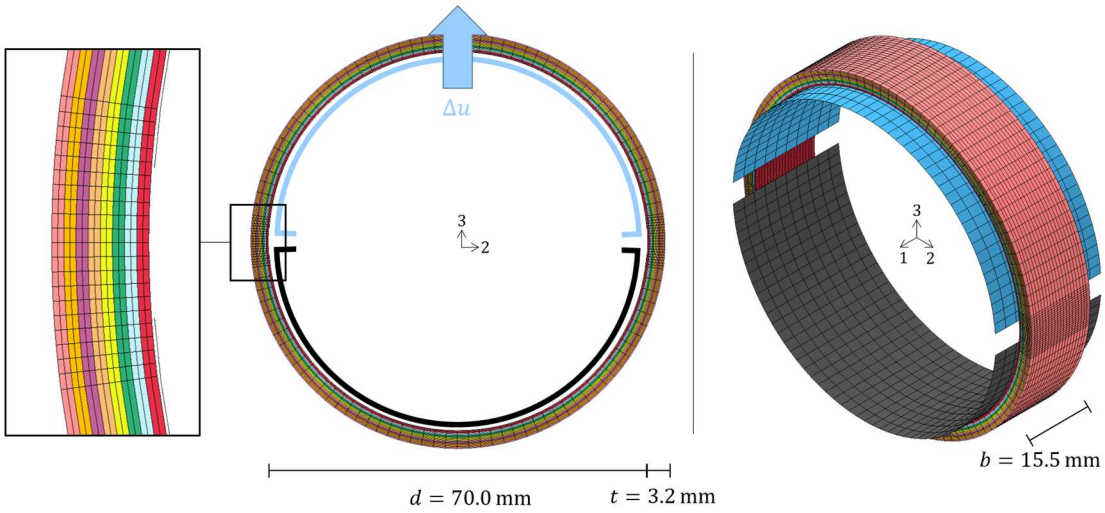

Fig.6: Stacked solid element simulation setup of the split disk test.

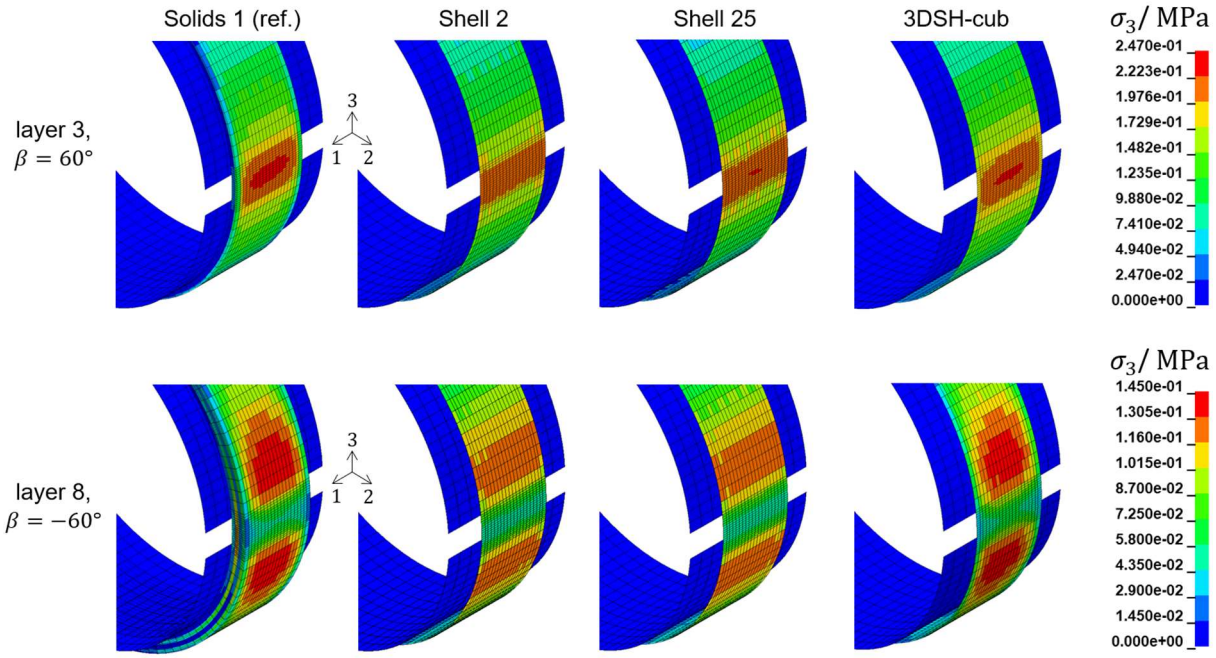

Fig.7: Distribution of normal stress σ_3 in the tensile direction around the equator of the laminate ring for layer 3 / integration point 6 (top row) and layer 8 / integration point 16 (bottom row) of the laminate for four different element formulations.

For the normal stress in σ_3 in layer 3, the reference solution with solid elements predicts a stress concentration of about $\sigma_3 = 0.247\ \mathrm{MPa}$ at the equator of the ring, which is slightly angled in direction of the fibers in this layer. The stress decreases both in the circumferential direction of the ring and in the direction of the free edges. Both standard shell elements, Shell 2 and Shell 25, correctly predict the approximate location of the stress maximum at the equator of the ring, but underestimate its magnitude. While these elements are able to correctly predict the decrease in stress in the circumferential direction, they again are unable to predict the stress decrease in the direction of the free edges. In contrast, the higher-order 3D-shell element predicts a stress distribution very close to the reference solution, capturing the stress maximum, the decay in circumferential direction, the decay towards the free edges, and the alignment of tensile stress with the fibers.

For layer 8, the outermost layer, the stress maximum in the reference solution is located slightly above and below the equator of the ring, again decreasing in circumferential direction and towards the free edges. In terms of their accuracy, the simulation results from the shell elements closely align with the results from layer 3. The standard shells again underestimate the stress maximum and are unable to predict the decrease towards the free edge, whilst the stress prediction from the higher-order 3D-shell element closely aligns with the reference solution.

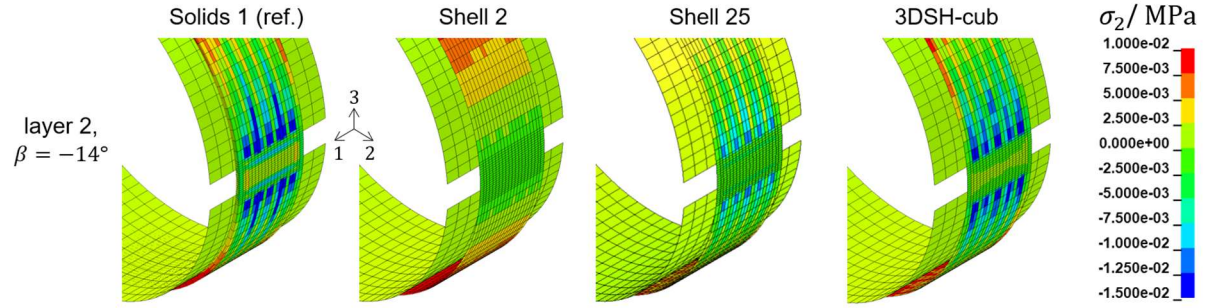

Fig.8: Distribution of transverse normal stress σ_2 around the equator of the laminate ring for layer 2 / integration point 4 of the laminate for four different element formulations.

Lastly, Figure 8 shows the distribution of transverse normal stress σ_2 at the equator of the ring. The reference solution shows some compressive stress concentrations above and below the equator. These arise from the rigid tools, compressing the laminate. The oscillations stem from the very coarse mesh used for these tools and the contact formulation chosen. If these simulations were run again, using a finer mesh for the rigid tool would be advisable. Nonetheless, for the purpose of comparing the stress predictions from different element formulations, the chosen discretization with oscillations is sufficient. While Shell 2 is unable to capture the transverse normal stress σ_2, using Shell 25 gives a minor improvement. Shell 25 is able to predict the compressive stress arising from the contact with the tools but underestimates its magnitude. This closely aligns with the results of an impact test conducted in [5]. Also, for this stress component, using a higher-order 3D-shell element greatly improves the accuracy of the stress prediction for the laminate. Both the location and magnitude of the compressive stress concentrations are captured almost exactly, using just a fraction of the degrees of freedom of the reference simulation with solid elements.

5 Summary and outlook

In conclusion, our contribution highlights a promising and viable approach to achieve more reliable stress predictions for composite structures in Ansys LS-DYNA, crucial for robust design and damage assessment, without the prohibitive cost of fully three-dimensional discretization.

The enhanced predictive capability of a higher-order 3D-shell element for stress in laminated composites is demonstrated for two scenarios at different scales. Results from numerical tests indicate that the cubic 3D-shell element (3DSH-cub) is much more accurate than Reissner–Mindlin shell elements (Shell 2) in representing the stress in laminated composites. The use of shell elements incorporating a thickness stretch (Shell 25) is only marginally beneficial if transverse stress arises due to contact. Otherwise, the shell elements with thickness stretch predict very similar stress distributions as the Reissner–Mindlin shell elements, underestimating the magnitude of stress at stress concentrations and excluding any effects of free edges on the stress distribution. In contrast, the simulation results from the cubic 3D-shell elements are more closely aligned with those of fully three-dimensional simulations with solid elements while being computationally more efficient due to being a shell formulation. As demonstrated in [13], the cubic 3D-shell element reduces computing time per time step by approximately 50 % compared to five solid elements across the thickness of the same model. For a comprehensive comparison of the numerical efficiency of the different element formulations, refer to [13].

This contribution allows for further investigation into the potential of higher-order 3D-shell elements to accurately capture the mechanical behavior of laminated materials. Especially investigations into the prediction of damage, load-bearing behavior after damage, and the influence of the transverse integration rule on the stress prediction seem sensible.

On the other hand, this contribution also shows that further improvements in the stress prediction might be possible to reduce the stress oscillations found in the detailed analysis of a laminate. One possible approach could be the enhancement of the higher-order 3D-shell elements with the capacity to model discontinuities in the transverse direction.

6 Acknowledgement

We gratefully acknowledge the support for this research from the DigiTain project (19S22006K), funded by the Federal Ministry of Economic Affairs and Energy, following on a resolution of the German Bundestag.

Funded by the European Union
NextGenerationEU

Gefördert durch:
Bundesministerium für Wirtschaft und Energie
aufgrund eines Beschlusses des Deutschen Bundestages

7 Appendix

For all finite element simulations in this contribution, an orthotropic material model with optional brittle failure for fiber-reinforced composites (***MAT_022** / ***MAT_COMPOSITE_DAMAGE**) is employed. Table 1 provides the material card used in the simulation of the tensile test in Section 4.1. For a detailed explanation of the parameters, see [14]. The values for all parameters were calculated from the values given by Pagano [15]; failure is excluded.

Table 2 provides the material card used for the simulations of the split disk test in Section 4.2. The values for all parameters were provided by project partners in the DigiTain project.

mid	**ro**	**ea**	**eb**	**ec**	**prba**	**prca**	**prcb**
1	1.8E-9	137895.15	14478.99	14478.99	0.02205	0.02205	0.21
gab	**gbc**	**gca**	**kfail**	**aopt**	**macf**	**atrack**	
5860.5436	5860.5436	5860.5436	0.0	2.0	1	0	
xp	**yp**	**zp**	**a1**	**a2**	**a3**		
0.0	0.0	0.0	1.0	0.0	0.0		
v1	**v2**	**v3**	**d1**	**d2**	**d3**	**beta**	
0.0	0.0	1.0	0.0	1.0	0.0	0.0	
sc	**xt**	**yt**	**yc**	**alph**	**sn**	**syz**	**szx**
0.0	0.0	0.0	0.0	0.0	0.0	0.0	0.0

Table 1: Material card for ***MAT_022** *used in the simulations of the tensile test.*

mid	**ro**	**ea**	**eb**	**ec**	**prba**	**prca**	**prcb**
2	1.8E-6	145.9	8.831	8.831	0.017	0.017	0.28
gab	**gbc**	**gca**	**kfail**	**aopt**	**macf**	**atrack**	
3.67	2.854	3.67	0.0	3.0	0	0	
xp	**yp**	**zp**	**a1**	**a2**	**a3**		
0.0	0.0	0.0	0.0	0.0	0.0		
v1	**v2**	**v3**	**d1**	**d2**	**d3**	**beta**	
1.0	1.0	1.0	0.0	0.0	0.0	0.0	
sc	**xt**	**yt**	**yc**	**alph**	**sn**	**syz**	**szx**
0.0	0.0	0.0	0.0	0.0	0.0	0.0	0.0

Table 2: Material card for ***MAT_022** *used in the simulations of the split disk test.*

8 Literature

[1] Mallick, P.K.: "Fiber-reinforced composites: materials, manufacturing, and design", CRC press, 2007.

[2] Främby, J., Brouzoulis, J., Fagerström, M., & Larsson, R.: "Prediction of through-thickness stress distribution in laminated shell structures", In *Proceedings of NSCM-27: the 27th Nordic Seminar on Computational Mechanics*, 2014.

[3] Czichos, R., Bergmann, T., Moldering, F., & Middendorf, P.: "Comparison of numerical modelling approaches for the residual burst pressure of thick type IV composite overwrapped pressure vessels related to low-velocity impact", *International Journal of Pressure Vessels and Piping 199 104770*, 2022.

[4] Willmann, T.: "3D-shell element technology, nonlinear poisson stiffening and data-integrated time step estimation", PhD thesis, University of Stuttgart, Institute for Structural Mechanics, 2025.

[5] Schilling, M., Usta, T., Willmann, T., von Scheven, M., & Bischoff, M.: "Investigating the Potential of Higher-Order 3D-Shell Finite Elements in Stress Analysis of Laminated Structures". In *Stuttgart Conference on Automotive Production*. Springer Nature Switzerland, 2024, pp. 1-12.

[6] Bischoff, M., Bletzinger, K. U., Wall, W. A., & Ramm, E.: "Models and finite elements for thin-walled structures". *Encyclopedia of computational mechanics*, 2004.

[7] Ansys, Inc.: "ANSYS LS-DYNA Keyword User's Manual Volume I", version (09/10/25), https://ftp.lstc.com/anonymous/outgoing/web/ls-dyna_manuals/DRAFT/DRAFT_Vol_I.pdf, accessed 01 October 2025, 2025.

[8] Belytschko, T., Lin, J. I., Tsay, C.-S.: "Explicit algorithms for the nonlinear dynamics of shells", *Computer Methods in Applied Mechanics and Engineering*, *42*(2), 1983, 225-251.

[9] Carrera, E., Valvano, S., Filippi, M.: "Classical, higher-order, zig-zag and variable kinematic shell elements for the analysis of composite multilayered structures", *European Journal of Mechanics-A/Solids, 72*, 2018, 97-110.

[10] Kühhorn, A., Schoop, H.: "A nonlinear theory for sandwich shells including the wrinkling phenomenon", *Archive of Applied Mechanics*, *62*(6), 1992, 413-427.

[11] Parisch, H.: "A continuum-based shell theory for non-linear applications", *International Journal for Numerical Methods in Engineering*, *38*(11), 1995, 1855-1883.

[12] Wessel, A., Butz, A., Schilling, M., Willmann, T., Bischoff, M.: "*Verbesserte Blechumform-simulation durch 3D-Werkstoffmodelle und erweiterte Schalenformulierungen-Teil 2*", AiF-Nr.: 21466N, EFB-Nr.: 06/219. Europäische Forschungsgesellschaft für Blechverarbeitung e.V. (EFB). ISBN: 978-3-86776-676-0, 2024.

[13] Schilling, M., Willmann, T., Wessel, A., Butz, A., Bischoff, M.: "Higher-order 3D-shell elements and anisotropic 3D yield functions for improved sheet metal forming simulations: part I", In *European LS-DYNA Conference 2023*, 2023.

[14] Ansys, Inc.: "ANSYS LS-DYNA Keyword User's Manual Volume II Material Models", version (09/10/25), https://ftp.lstc.com/anonymous/outgoing/web/ls-dyna_manuals/DRAFT/DRAFT_Vol_II.pdf, accessed 01 October 2025, 2025.

[15] Pagano, N. J.: "Free edge stress fields in composite laminates", *International Journal of Solids and Structures*, *14*(5), 1978, 401-406.

[16] ASTM International: "Standard Test Method for Apparent Hoop Tensile Strength of Plastic or Reinforced Plastic Pipe", D2290–19a, 2019.